

# Long-Range Ambient LoRa Backscatter with Parallel Decoding

Jinyan Jiang, Zhenqiang Xu, Fan Dang, Jiliang Wang  
School of Software and BNRist, Tsinghua University, Beijing, P.R. China  
{jiangjy20, xu-zq17}@mails.tsinghua.edu.cn, {dangfan, jiliangwang}@tsinghua.edu.cn

## ABSTRACT

LoRa backscatter is a promising technology to achieve low-power and long-distance communication for connecting millions of devices in the Internet of Things. We present P<sup>2</sup>LoRa, the first ambient LoRa backscatter system with parallel decoding and long-range communication. The high level idea of P<sup>2</sup>LoRa is to modulate data by shifting ambient LoRa packets with a small frequency. To achieve long distance communication, we enhance the SNR of the backscatter signal by concentrating leaked energy in both the frequency domain and time domain. We propose a method to accurately reconstruct and cancel the in-band excitation signal, which is orders of magnitude higher than the backscatter signal. For parallel decoding, we propose a method to cancel inter-tag interference with very low overhead and address the signal misalignment problem due to different time of flight. We prototype the P<sup>2</sup>LoRa tag with customized low-cost hardware and implement the P<sup>2</sup>LoRa gateway on USRP. Through extensive evaluations, we show that P<sup>2</sup>LoRa achieves a long communication distance of 2.2 km with ambient LoRa, and supports 101 parallel tag transmissions.

## CCS CONCEPTS

• Networks → Network protocols; • Computer systems organization → Embedded and cyber-physical systems.

## KEYWORDS

Backscatter, LoRa, Parallel Decoding

### ACM Reference Format:

Jinyan Jiang, Zhenqiang Xu, Fan Dang, Jiliang Wang. 2021. Long-Range Ambient LoRa Backscatter with Parallel Decoding. In *The 27th Annual International Conference on Mobile Computing and Networking (ACM MobiCom '21)*, October 25–29, 2021, New Orleans, LA, USA. ACM, New York, NY, USA, 13 pages. <https://doi.org/10.1145/3447993.3483261>

## 1 INTRODUCTION

Recent advances in backscatter systems bring low power, low cost, small form factor to wireless communication. Among them, LoRa backscatter is considered a promising technology as it overcomes the short communication distance of the traditional backscatter systems. By leveraging LoRa modulation and demodulation features,

Permission to make digital or hard copies of all or part of this work for personal or classroom use is granted without fee provided that copies are not made or distributed for profit or commercial advantage and that copies bear this notice and the full citation on the first page. Copyrights for components of this work owned by others than ACM must be honored. Abstracting with credit is permitted. To copy otherwise, or republish, to post on servers or to redistribute to lists, requires prior specific permission and/or a fee. Request permissions from [permissions@acm.org](mailto:permissions@acm.org).  
*ACM MobiCom '21, October 25–29, 2021, New Orleans, LA, USA*

© 2021 Association for Computing Machinery.  
ACM ISBN 978-1-4503-8342-4/21/10...\$15.00  
<https://doi.org/10.1145/3447993.3483261>

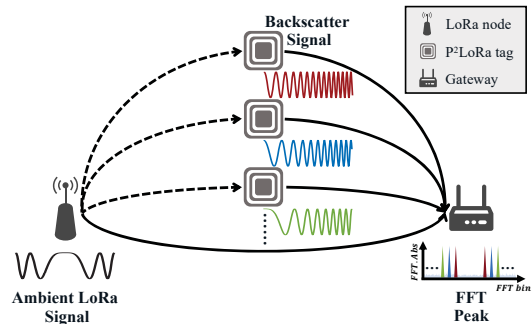


Figure 1: P<sup>2</sup>LoRa overview.

LoRa backscatter can increase the communication distance (*e.g.*, to hundreds of meters or even longer) while ensuring low power consumption. Thus, it has been shown as an important technology to connect the ever increasing devices in the Internet of Things and support various applications such as smart agriculture, smart city, and smart healthcare [1–4].

There emerges an extensive collection of LoRa backscatter techniques, with representative ones shown in Table 1. Existing works, however, have the following limitations: **1) Dedicated excitation signal.** The LoRa backscatter [5] uses a dedicated single-tone RF source as an excitation signal to generate a LoRa-like backscatter signal. Netscatter [6] also uses a dedicated single-tone RF source instead of ambient LoRa. The wireless channel in LoRaWAN [9] is crowded and using a dedicated signal source incurs additional deployment and maintenance costs. It is better to use ambient LoRa signal to avoid additional spectrum overhead. **2) No parallel decoding.** One essential application scenario for backscatter technology is to provide data communication for many small objects without batteries for the Internet of Things. However, the LoRa backscatter [5], PLoRa [7] and Aloha [8] only work for a single or very few parallel backscatter packets. They cannot decode multiple backscatter packets simultaneously and thus fail to support communication for multiple devices. Netscatter [6] can decode parallel packets. However, it requires a specially designed excitation signal. In practice, it is essential to decode parallel backscatter packets especially considering the large communication range of LoRa. **3) Complex backscatter modulation.** Complex tag design incurs high power consumption and high hardware costs, which also makes reproducing and deploying the backscatter system difficult. The LoRa backscatter [5] requires generating linearly increasing frequency, which needs a high precision voltage-controlled oscillator (VCO) to control the shifting frequency. PLoRa [7] requires shifting signal by two different frequency offsets, and thus PLoRa tag is implemented based on FPGA. In summary, we can see that

**Table 1: Comparison with existing LoRa backscatter systems.**

	Backscatter range	Ambient RF source	Parallel decoding	Spectrum consumption	Compatible with COTS tags
LoRa backscatter [5]	2.8 km <sup>1</sup>	✗	✗	Medium	✗
Netscatter [6]	-	✗	✓	Low	✗
PLoRa [7]	1.1 km	✓	✗	High	✗
Aloba [8]	250 m	✓	< 6 tags <sup>2</sup>	Low	✓
<b>P<sup>2</sup>LoRa</b>	2.2 km	✓	✓ (> 100 tags)	<b>Low</b>	✓

<sup>1</sup> It uses 31.25 kHz BW and 6 dBi antenna while ours uses 500 kHz BW and 4 dBi antenna.

<sup>2</sup> The performance significantly degrades even under six tags according to their evaluation [8].

none of the existing works can achieve parallel backscatter with ambient LoRa signal based on low-cost hardware platforms.

This paper presents the **Passive and Parallel LoRa (P<sup>2</sup>LoRa)**, the first ambient LoRa backscatter supporting parallel decoding and long-range communication simultaneously. As shown in Figure 1, P<sup>2</sup>LoRa takes the ambient LoRa sent by COTS LoRa devices as the excitation signal. The main idea of P<sup>2</sup>LoRa tag is to shift the LoRa signal with a certain small frequency offset to encode data in the backscatter signal. The LoRa gateway receives the backscatter signal from multiple P<sup>2</sup>LoRa tags along with the original LoRa signal, and then it decodes multiple backscatter signals as well as the original LoRa signal, simultaneously. A P<sup>2</sup>LoRa tag only needs to shift the frequency of the excitation signal, and thus it has very low hardware complexity and is compatible with COTS backscatter tags such as WISP [10].

Turning the basic idea of P<sup>2</sup>LoRa into reality needs to address the following challenges:

*First, how to decode the backscatter signal with unknown excitation signal and enhance its SNR for long-range communication?* The ambient LoRa signal carries encoded data, which is unknown for backscatter tags. To convey data bits, a P<sup>2</sup>LoRa tag shifts the ambient LoRa signal with a certain frequency  $f_{shift}$  to encode the data bits. This frequency shifting operation is typically based on multiplying a square wave which is easy to generate on tag, and this operation leads to mirror copies of backscatter signals. Traditional approaches such as PLoRa only exploit one copy of them while ignoring others, which significantly degrades the SNR. We leverage the excitation signal as the reference and propose a switch-and-splice method to transform the unknown ambient LoRa chirp to a base up-chirp with linearly increasing frequency from  $f_{shift}$  to  $f_{shift} + BW$ , where  $BW$  is the chirp bandwidth. Then, as the backscatter modulation spreads the energy to different copies in double sidebands, we propose a method to combine the energy in double sidebands to enhance the SNR. Compared with existing approaches, our design concentrates the energy of the whole backscatter symbol across double sidebands and improves the signal SNR. This enhances the communication range by 67% under the same bit error rate (BER). We also present a detailed analysis for the SNR and range improvement in Section 7.1.

*Second, how to decode the backscatter signal in the presence of the in-band excitation signal, which is typically orders of magnitude higher?* In P<sup>2</sup>LoRa, the backscatter signal overlaps with the

excitation signal. This improves spectrum efficiency, minimizes its interference to other channels, and reduces the tag hardware complexity for frequency shifting. However, this also brings challenges for canceling the excitation signal. Reconstructing and canceling the excitation LoRa signal requires accurate signal parameters such as phase, start frequency and amplitude. We propose a two-level parameter estimation method. We first leverage the up-down chirp structure in the LoRa packet to find the coarse parameters of the LoRa chirp. Then, we propose a novel fitting-based method to refine those parameters to sub-sample level, which enables us to precisely reconstruct and cancel the excitation signal. After canceling the interference from excitation signal, P<sup>2</sup>LoRa reduces the average BER by 75% under different communication distances.

*Third, how to decode parallel backscatter signals?* 1) It is difficult to cancel inter-tag interference, especially for a large number of tags. 2) Backscatter signal is typically very weak, making it further difficult to decode. 3) Different backscatter packets may not align in time due to different distances from tags to the gateway. We propose an efficient window-based signal separation method using a combined Hanning window to mitigate inter-tag interference and decode multiple parallel backscatter packets. As a result, P<sup>2</sup>LoRa achieves parallel backscatter of 101 tags. Compared with PLoRa [7], P<sup>2</sup>LoRa achieves 16.3× higher throughput.

In summary, the main results and contributions are as follows:

- We propose P<sup>2</sup>LoRa, the first ambient LoRa backscatter with parallel decoding for long-range communication. We design a method to concentrate the backscatter signal's energy and enhance its SNR to improve the communication range. We propose a novel method to reconstruct and cancel the original excitation LoRa signal accurately. Finally, we propose a window-based method to cancel the interference among weak backscatter signals to achieve parallel decoding.
- We prototype P<sup>2</sup>LoRa tag on a customized PCB board using commercial low-cost off-the-shelf circuit components and implement P<sup>2</sup>LoRa gateway on USRP. P<sup>2</sup>LoRa can be seamlessly embedded in the current LoRa network. We evaluate P<sup>2</sup>LoRa performance extensively in different scenarios. The evaluation results show that P<sup>2</sup>LoRa achieves a 2.2 km communication distance when the tag is close to the RF source and support parallel decoding for 101 tags.

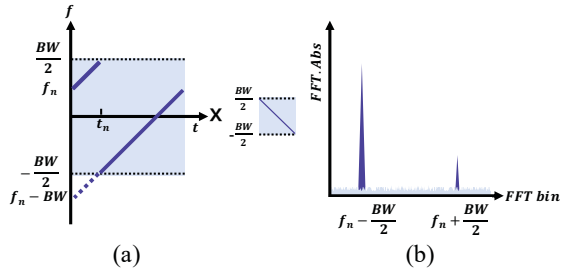


Figure 2: Basic LoRa demodulation via multiplying a down-chirp and applying FFT.

## 2 LORA PRIMER

LoRa adopts the CSS (Chirp Spreading Spectrum) mechanism to encode data. The basic unit in LoRa is a linear chirp whose frequency changes linearly with time. An up-chirp/down-chirp has frequency increasing/decreasing with time. LoRa has a parameter SF (Spreading Factor) to control the slope of the chirp, defined as

$$2^{SF} = BW \cdot T,$$

where  $BW$  is bandwidth and  $T$  is chirp length. An up-chirp in baseband can be expressed as

$$c(t; f_0) = e^{j2\pi(f_0 t + \frac{1}{2} k t^2)}, \quad 0 \leq t \leq T,$$

where  $f_0$  is the initial frequency and  $k = \frac{BW}{T}$  is the frequency changing rate. An up-chirp is a base up-chirp if  $f_0 = -\frac{BW}{2}$ . For simplicity, we denote the base up-chirp as  $c(t) = c(t; -\frac{BW}{2})$ . A LoRa symbol is a cyclicly shifted version of the base up-chirp, which can be expressed as

$$s(t; f_n) = c(t; f_n)w(t; 0, t_n) + c(t; f_n - BW)w(t; t_n, T),$$

where  $f_n = -\frac{BW}{2} + n \cdot \frac{BW}{2^{SF}}$  ( $n = 0, 1, \dots, 2^{SF} - 1$ ) is the start frequency of the LoRa symbol,  $t_n = T - n \cdot \frac{T}{2^{SF}}$  and  $w(t; t_a, t_b)$  is a rectangular function whose definition is

$$w(t; t_a, t_b) = \begin{cases} 1, & t_a \leq t < t_b; \\ 0, & \text{otherwise.} \end{cases}$$

There are  $2^{SF}$  choices of  $f_n$  for the start frequency of a LoRa symbol to encode  $SF$  bits. To decode, we extract the value of  $f_n$  from a LoRa symbol on the receiver side by *dechirp*: 1) We first multiply it with a base down-chirp  $c^*(t)$ , i.e., the conjugate of a base up-chirp,

$$\begin{aligned} s'(t; f_n) &= s(t; f_n) \cdot c^*(t) \\ &= e^{j2\pi(f_n + \frac{BW}{2})t} w(t; 0, t_n) + e^{j2\pi(f_n - \frac{BW}{2})t} w(t; t_n, T) \end{aligned}$$

2) Then, we apply FFT on  $s'(t; f_n)$  and derive frequency peaks  $f_n \pm \frac{BW}{2}$  in frequency domain, which indicates the encoded  $SF$  bits, as shown in Figure 2.

## 3 DESIGN OVERVIEW

**Design Goals.** The design of P<sup>2</sup>LoRa is driven by the following goals.

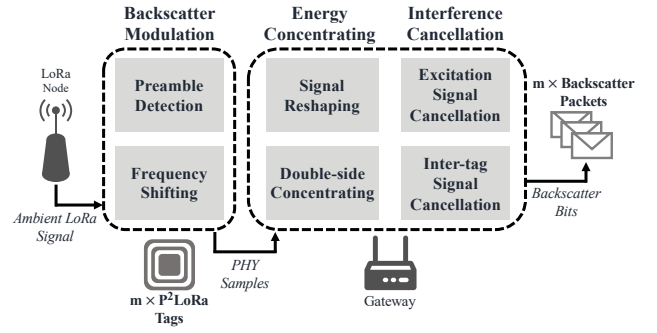


Figure 3: The main workflow of P<sup>2</sup>LoRa.

- Ambient RF source. Using a dedicated RF source incurs additional system overhead and also occupies the spectrum. Our goal is to take the ambient LoRa transmission as the excitation signal.
- Minimize SNR loss. We leverage the feature of LoRa and minimize the SNR loss to achieve long-range backscatter.
- Parallel backscatter. As an ultra low power device, the backscatter tag cannot run complex MAC-layer protocols. We aim to design a parallel backscatter system to share the spectrum with multiple tags and decode simultaneous packet transmissions.
- Minimize spectrum consumption. Traditional approaches shift the excitation signal to a distant frequency to avoid interference. We share the spectrum between the excitation signal and the backscatter signal to minimize spectrum consumption.
- Simple tag hardware. The operations on tags should be simple (e.g., avoid generating complex signals like FMCW as in [5]) to reduce the tag cost and complexity.

Figure 3 illustrates the workflow of P<sup>2</sup>LoRa design:

**Backscatter Modulation.** P<sup>2</sup>LoRa leverages the ambient LoRa as the excitation signal, which is unpredictable for tags. Therefore, a P<sup>2</sup>LoRa tag in Figure 3 first detects the ongoing LoRa packet and synchronizes with it. Upon detecting the ambient LoRa transmission, the tag enters the data modulation phase. Each tag uses  $n$ -Frequency Shift Keying ( $n$ -FSK) to encode data bits. The  $k^{\text{th}}$  tag conveys different symbols by shifting the excitation signal by frequency  $\Delta f_1^k, \Delta f_2^k, \dots, \Delta f_n^k$ . The length of an FSK symbol sent by tags is the same with the excitation symbol. The frequency shifting is accomplished by generating a square wave baseband signal at the tag (The state-of-the-art method [5] can be used to eliminate the harmonics of the square wave). The shifting frequency  $\Delta f$  is set to be less than the chirp bandwidth  $BW$  to minimize spectrum consumption. For example, a tag using 2-FSK can encode “0” or “1” by shifting the excitation signal by  $\Delta f_1^1 = \frac{BW}{2}$  or  $\Delta f_2^1 = \frac{BW}{2} - \frac{BW}{2^{SF}}$ . We only require a small baseband signal frequency at the tag, which reduces the tag power consumption and interference to the adjacent frequency band.

**Backscatter energy concentrating.** Then, the gateway can obtain the hybrid signal consisting of the excitation signal and backscatter signals from different tags. The main purpose of decoding is to derive the shifting frequency of the backscatter signal for different tags. To decode the hybrid signal, the gateway first

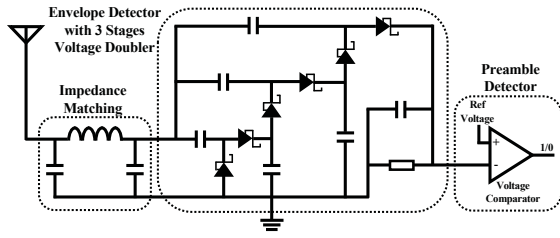


Figure 4: Ambient LoRa Signal Detection Circuit.

performs a standard packet detection to synchronize with the excitation signal coarsely. Then, it sets the reception window aligning with chirps of excitation signal and decodes both the excitation signal and backscatter signal by symbol. To generate the backscatter signal, the P<sup>2</sup>LoRa tag uses a real baseband signal for frequency shifting. Therefore, during the backscatter process, two copies (image copy and real copy, *a.k.a.*, upper and lower sidebands) are generated in the frequency domain. We design a signal reshaping method to concentrate the energy of backscatter signals to a single-tone. To maximize the peak height after FFT, P<sup>2</sup>LoRa also concentrates the energy of the double sidebands.

**Parallel decoding and interference cancellation.** For parallel decoding, we need to address two key challenges. First, we need to cancel the interference from the excitation signal, which is much stronger than the backscatter signal. Second, we need to cancel the inter-tag interference. For excitation signal cancellation, we perform accurate parameter estimation and eliminate the strongest signal. For inter-tag interference cancellation, intuitively we can iteratively cancel each the signal of each tag. In practice, it is very difficult to accurately estimate the parameters of the backscatter signal as the signal is typically very weak. Thus, we design a cancellation window function to reduce inter-tag interference. Then, we obtain robust peaks in the frequency domain and decode backscatter data packets by mapping those peaks to FSK symbols.

## 4 P<sup>2</sup>LORA BASIC DESIGN

We first introduce P<sup>2</sup>LoRa for a single tag, and then extend it to parallel decoding in the next section. Without loss of generality, assume the tag uses n-FSK modulation and the data bits are encoded by the shifting frequencies  $\Delta f_1, \Delta f_2, \dots, \Delta f_n$ .

### 4.1 Challenges

**Strong in-band interference.** To minimize spectrum consumption, the shifting frequency is much smaller than the bandwidth of the excitation signal  $BW$  (i.e.,  $\Delta f < BW$ ). Meanwhile, the backscatter signal is several orders of magnitude weaker than the excitation signal. Therefore, how to reduce the strong in-band interference is important and challenging.

**Low-cost hardware operations.** Due to limited hardware resources, the backscatter tag cannot perform standard LoRa packet detection. Besides, the low-cost/COTS hardware only supports a limited frequency shifting. A method like PLoRa requires two antennas and two baseband signals with accurate signal operations on FPGA.

**Concentrating backscatter energy.** While shifting the excitation signal, the low-cost backscatter tag generates two copies of signals at double sidebands. It is essential to concentrate the energy of those backscatter signals to minimize SNR loss.

In this section, we first introduce the tag basic hardware design and then the decoding processes to address the challenges.

### 4.2 P<sup>2</sup>LoRa Tag Design

Figure 4 illustrates the detection circuit design of P<sup>2</sup>LoRa tag. We use a low-power circuit to detect the incoming of the LoRa packet. This process does not require the MCU involvement, and thus supports a low power budget. To improve the receiving sensitivity, we design a three-stage voltage doubler circuit to boost the incoming voltage to the comparator, which can achieve a sensitivity at  $-49.5$  dBm and translates to a waking-up distance of 104 m. To accurately identify the LoRa preamble, Aloba [8] adds a band-pass filter before the envelope detector, and then checks the characteristics of the LoRa data packet in the frequency domain. In our work, we can also add a similar band-pass filter to the tag to achieve accurate packet identification. The typical hardware delay of the waking-up circuit is at the level of several  $\mu$ s. Given the length of a LoRa chirp (usually several milliseconds), the impact of delay on the communication performance is negligible.

At the tag, we need to generate the square wave baseband signal. Intuitively, we can use the microcontroller to generate the PWM waveform. However, this can only set the frequency division ratio to the power of two, leading to a coarse frequency shifting. Thus, we use a low-power DAC and VCO to generate the square wave baseband signal. As we only need to shift the signal by a small frequency offset, we use a less accurate VCO to lower the power consumption.

### 4.3 Concentrating Single Sideband Energy

Upon detecting the ambient LoRa signal, a P<sup>2</sup>LoRa tag shifts the incoming LoRa symbol by different frequencies to convey backscatter bits. As shown in Figure 5(a), the frequency shifting process generates two copies (lower and upper sidebands) of the backscatter signal. The backscatter signal together with the excitation signal are received at the gateway. Assume the maximum shifting frequency is  $\Delta f_n = \frac{BW}{2}$ . The maximum frequency of the received hybrid signal is  $\frac{BW}{2} + \frac{BW}{2} = BW$ . Accordingly, we set the sampling rate to  $2BW$  (blue area in Figure 5(a)).

When the excitation signal is a normal chirp (as shown in Figure 5(b)), by applying dechirp and FFT to the received signal, we can obtain four FFT peaks in the frequency domain: two for the upper sideband, and two for the lower sideband. Therefore, the total energy of the received signal is distributed to four peaks. We need to concentrate the energy for those peaks to improve SNR for decoding. When the excitation signal is a base up-chirp, *i.e.*, a chirp with linearly increasing frequency from  $\frac{BW}{2}$  to  $-\frac{BW}{2}$ , there are only two peaks corresponding to the backscatter chirps in the FFT domain as shown in Figure 5(c) and Figure 5(d). In such a case, the energy of a single sideband is concentrated to a single peak. Each peak is twice as high as the one for that of the normal chirp.

In reality, the excitation signal is normal chirps with different starting frequencies rather than base up-chirps. Our key idea is to

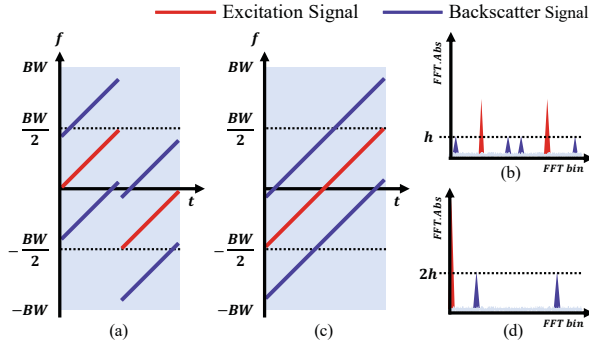


Figure 5: Dechirp and FFT on the received signal: (a)(b) Demodulation result of a normal chirp symbol. (c)(d) Demodulation result of a base chirp symbol.

transform the received excitation signal and backscatter signal to base up-chirp. As the excitation signal is typically stronger than the backscatter signal [11], we first decode the excitation signal by tracking the highest peak after FFT. After decoding the excitation signal, we obtain the starting frequency of the excitation signal. We can also calculate  $t'$  from Figure 6, which corresponds to the position that a chirp reaches its highest frequency. Based on this information, as shown in Figure 6, we propose a switch and splice method to transform a normal chirp to the base up-chirp.

We first divide the received chirps into two parts: the part before  $t'$  and the part after  $t'$ . Then, we switch these two parts and splice them to form a new signal. As we can see from Figure 6, this intuitively results in a base up-chirp. However, the resulted base up-chirp is not a perfect one. There exists a phase discontinuity, *i.e.*, a phase offset, at the splicing position  $t'$  for a LoRa chirp [12]. The phase discontinuity is inherently due to the LoRa modulation mechanism [13]. It is nondeterministic and occurs at the point of chirp moving from the highest frequency to the lowest. The phase discontinuity reduces the peak height as well as the SNR after dechirp in demodulation as two parts of the sub-chirps add destructively. Such a problem is ignored in existing approaches, *e.g.*, in PLoRa, and leads to a significant SNR loss. Ideally, we can search for the phase offset and compensate for it. However, this incurs a very high computation overhead to test for different phase offsets (from 0 to  $2\pi$ ).

To address this problem, we propose a simple but effective method. First, we compensate the phase discontinuity by  $\pi$  for the phase of the sampling point right after  $t'$ . Then, we perform FFT on the signals before and after compensation and then take the larger peak value. Assume the initial phase offset due to phase discontinuity is  $\phi$ . The phase offset after compensation is  $\min(\phi, \phi - \pi)$ , which should be smaller than  $\frac{\pi}{2}$ . Clearly, compensating the phase discontinuity by more phases (*e.g.*,  $\frac{\pi}{2}, \pi, \frac{3\pi}{2}$ ), we can obtain a signal with a smaller phase offset and achieve better compensation (*e.g.*,  $\frac{\pi}{4}$ ) at the cost of a higher computation overhead. This leads to a trade-off between computation overhead and compensation performance.

PLoRa uses signals in two basebands with no phase synchronization and then splice them to generate a backscatter chirp. Therefore, the phase discontinuity occurs twice in PLoRa, *i.e.*, at the

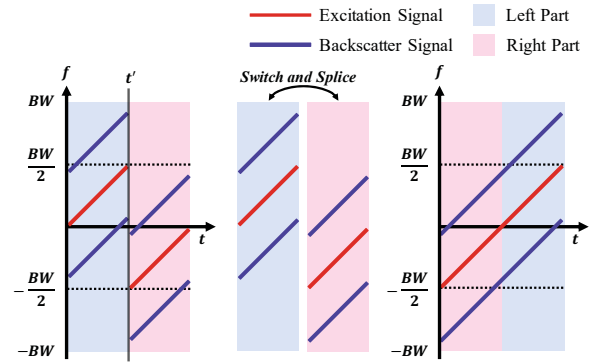


Figure 6: Switch and splice the left and right parts to get the base up-chirp.

position of splicing and at the position of reaching the maximum frequency [12]. Due to the phase discontinuity, PLoRa cannot effectively concentrate the energy of the whole chirp. To demonstrate the SNR improvement of the phase compensation in our design, we conduct a comparative experiment with PLoRa. In our experiments, the backscatter signal strength of P<sup>2</sup>LoRa and PLoRa is the same. The only difference is that P<sup>2</sup>LoRa compensates the phase discontinuity while PLoRa does not. The initial frequency of the excitation signal and the phase offset are set randomly. We measure the height of backscatter peaks after dechirp and FFT, then calculate the SNR loss for P<sup>2</sup>LoRa and PLoRa compared to the ideal case (*i.e.*, without any phase discontinuity). The SNR loss of our method is around 0.25 dB; without compensation, the SNR loss of PLoRa is around 2.05 dB. Thus, our method provides 1.8 dB SNR gain compared with PLoRa.

In our design, the switch and splice window are aligned with the excitation signal as we assume the excitation signal and backscatter signal arrive at the gateway at the same time. In practice, since the backscatter signal typically arrives at the gateway later than the excitation signal due to different Time of Flight (ToF). For example, when the distance from tags to the source is 150 m, the maximum ToF difference between the excitation signal and the backscatter signal can be calculated as  $\Delta t = \frac{2 \cdot 150m}{3 \cdot 10^8 m/s} = 10^{-6} s$ . The time offset caused by different ToF is smaller than the sampling interval (*e.g.*, the sampling interval is 1  $\mu s$  for a chirp with bandwidth 500 kHz and 1 MHz sampling rate). Thus, the time offset should not introduce a significant impact on the performance of switch and splice.

#### 4.4 Concentrating Double Sideband Energy

A typical backscatter signal uses a square wave to shift the frequency of excitation signal  $c(t)$ . The square wave can be approximated to a real single frequency signal  $\cos(\Delta ft)$ , which results in two sidebands in the frequency domain:

$$\begin{aligned}
 c(t) \cdot \cos(\Delta ft) &= c(t) \cdot \frac{1}{2} \left( e^{j2\pi\Delta ft} + e^{-j2\pi\Delta ft} \right) \\
 &= \underbrace{\frac{1}{2} c(t) e^{j2\pi\Delta ft}}_{\text{upper sideband}} + \underbrace{\frac{1}{2} c(t) e^{-j2\pi\Delta ft}}_{\text{lower sideband}} \quad (1)
 \end{aligned}$$

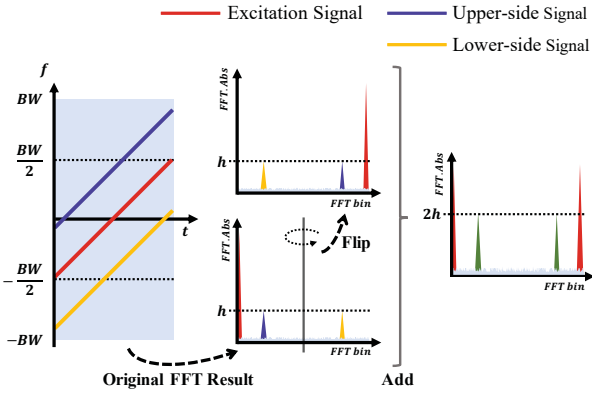


Figure 7: Flip the ABS result of FFT and add to the original result.

Previous works either eliminate the lower sideband [14] or only utilize the upper sideband [7]. To generate a single sideband backscatter signal, the hardware complexity of the tag is much higher, e.g., capable of generating a negative lower sideband. We adopt a very simple tag design to reduce hardware complexity and power consumption and make the tag be compatible with COTS backscatter tags. Therefore, the backscatter signal has double sidebands. After switching and splicing, those two sidebands are transformed into two peaks in the frequency domain. To leverage those two sidebands, as shown in Figure 7, we calculate the absolute value of the FFT result and add up the peaks non-coherently before and after flipping the FFT sequence. In this way, the backscatter energy of the upper and lower sidebands is concentrated. However, this leads to two practical problems. First, the noise is also added up. The backscatter peak is coherently enhanced while the noise is randomly added. Thus, two backscatter peaks should be more prominent after adding up.

The second problem is due to different ToF for different tags. The position of peaks for the upper sideband may not be exactly the same with that of the lower sideband after flipping. As mentioned in Section 4.3, the backscatter signal arrives at the gateway  $\Delta t$  seconds later than the excitation signal. Denote the upper and lower sidebands as  $b_{upper}(t) = c(t - \Delta t) \cdot e^{j2\pi\Delta f t}$  and  $b_{lower}(t) = c(t - \Delta t) \cdot e^{-j2\pi\Delta f t}$ , respectively. After dechirp, the delay in the time domain can be translated into a frequency misalignment in the frequency domain:

$$\begin{aligned}
 & (b_{upper}(t) + b_{lower}(t)) \cdot c^*(t) \\
 &= \left( e^{j2\pi\Delta f t} + e^{-j2\pi\Delta f t} \right) \cdot e^{j2\pi\left(f_0(t-\Delta t) + \frac{1}{2}k(t-\Delta t)^2\right)} \cdot e^{-j2\pi\left(f_0 t + \frac{1}{2}k t^2\right)} \\
 &= \left( e^{j2\pi\left(\Delta f - \frac{\Delta t}{T}BW\right)t} + e^{j2\pi\left(-\Delta f - \frac{\Delta t}{T}BW\right)t} \right) \cdot e^{j2\pi\left(\frac{1}{2}k\Delta t^2 - f_0\Delta t\right)}
 \end{aligned} \tag{2}$$

The corresponding peaks after dechirp of the upper and lower sidebands are at frequency  $\Delta f_{upper} = \Delta f - \frac{\Delta t}{T}BW$  and  $\Delta f_{lower} = -\Delta f - \frac{\Delta t}{T}BW$ , respectively. We can see that those peaks are no longer symmetrical along  $f = 0$  in the frequency domain. Therefore, we cannot directly add those peaks. Directly folding and adding the misaligned peaks of FFT cannot provide the highest SNR. Assume

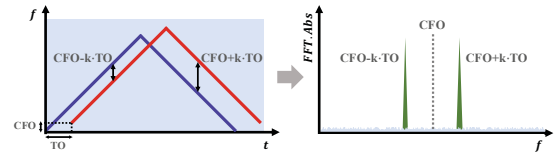


Figure 8: Coarse-grained estimation of CFO and TO.

the maximum ToF difference among tags is  $\Delta t = 10^{-6}$ s. Assume  $SF = 12$  and  $BW = 500$  kHz for the excitation signal, the ToF difference  $\Delta t$  translates to a frequency offset of  $\frac{\Delta t}{T} \cdot BW = 61$  Hz (0.5 FFT bins). Thus, instead of adding up the raw FFT result, we first zero-pad the original signal (e.g., to  $10\times$  of the original one) to capture the fine-grained FFT result and locate the exact position of the highest single-sideband peak. After padding, we divide every 10 FFT bins into one group, and calculate the maximum value in each group as the peak for the original bin before padding. By doing this, we obtain a new FFT sequence captures the highest peaks for the upper and lower sideband. Then we apply flipping and adding to the new sequence, which ensures the double sideband energy is concentrated even in presence of ToF delay.

#### 4.5 Excitation Signal Cancellation

The above operations are performed on the hybrid signal with the excitation signal. The excitation signal incurs severe interference to the much weaker backscatter signal. In P<sup>2</sup>LoRa, the backscatter signal overlaps with the excitation signal, which further exacerbates the interference. We utilize the feature that the excitation signal is much stronger than the backscatter signal. Thus, we propose a method to first reconstruct the excitation signal in the time domain and then cancel it from the hybrid signal. To reconstruct the excitation signal, we need to accurately estimate its parameters (including the frequency, amplitude, and initial phase). Meanwhile, we also need to accurately estimate the time offset (TO) and carrier frequency offset (CFO) of the excitation signal.

**Coarse-grained estimation.** As shown in Figure 8, we first leverage the packet structure of up-chirp and down-chirp in LoRa packets for coarse TO and CFO estimation [15]. In a LoRa packet, the preambles consists of base up-chirps and the SFD (Start of Frame Delimiter) consists of base down-chirps. After dechirp, the CFO shifts the peaks of the up-chirp and down-chirp by the same amount frequency. Therefore, when there is no TO, the peaks of base up-chirps and base down-chirps lie in the same FFT bin. The TO causes opposite frequency shifts for peaks of the up-chirp and down-chirp. According to Equation (2), the total shifted frequency of up-chirp is calculated as  $\delta f_{up} = CFO - \frac{TO}{T}BW$ . Similarly, for the base down-chirp, the shifted frequency is calculated as  $\delta f_{down} = CFO + \frac{TO}{T}BW$ . Based on the dechirp result of the up-chirp and the down-chirp, we can coarsely estimate the CFO and TO as:  $CFO = \frac{\delta f_{up} + \delta f_{down}}{2}$ ,  $TO = \frac{\delta f_{down} - \delta f_{up}}{2BW} \cdot T$ .

**Fine-grained estimation.** The above estimation relies on the accurate measurement of  $\delta f_{up}$  and  $\delta f_{down}$  by applying FFT to the dechirp result. The frequency accuracy is at most at the sampling point level as shown in Figure 9 (a). To further improve the accuracy of  $\delta f_{up}$  and  $\delta f_{down}$ , we first perform zero-padding on the dechirp

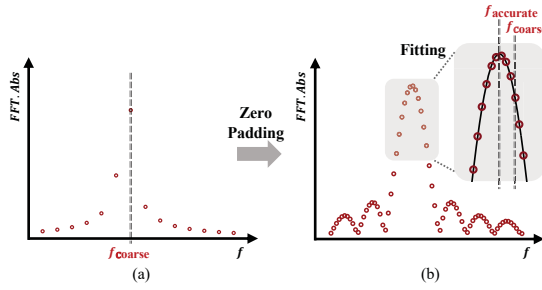


Figure 9: Fine-grained estimation of CFO and TO.

results of the up-chirp and down-chirp, respectively. After padding, we have multiple sampling points around the mainlobe, as shown in Figure 9 (b). Then, we perform nonlinear fitting on those sampling points around the mainlobe to obtain the height and frequency of the mainlobe. Note that the estimated frequency after padding is more accurate than the coarse-grained estimation result. Using the accurate peak corresponding to the up-chirp and down-chirp, we achieve the fractional level estimation of CFO and TO.

It is worth noting that the estimated CFO typically remains unchanged for a long period for the same transmitter and receiver pair. Therefore, the above process of CFO calculation does not need to be performed frequently and thus the estimation does not incur significant overhead.

Then, we can reconstruct the excitation signal and cancel it from the hybrid received signal. Then, we calculate the peaks for the remaining signal. As the peak corresponding to the backscatter signal may fall in  $n$  possible FFT bins, we check the ABS value of these  $n$  bins and map the highest peak to the backscatter bits.

## 5 PARALLEL DECODING

When there are  $n$  tags, it is expected to obtain  $n$  peaks in the frequency domain for those tags. Without loss of generality, we first consider the case of OOK for each tag. We show that our approach can also be extended to n-FSK for each tag. Intuitively, to decode multiple tags, we check the corresponding bin for each tag to see if there is a peak exceeding the threshold. If the answer is yes, the data bit for the tag is “1” and otherwise “0”. In practice, we need to address the following challenges.

**Inter-tag Interference.** The inter-tag interference makes the peak difficult to recognize. It is difficult to cancel the inter-tag interference due to the following reasons: 1) The power of the backscatter signal is typically several orders of magnitude weaker than the excitation signal, making it difficult to obtain the parameters such as frequency and phase of the backscatter signal. 2) The overhead of estimating and canceling inter-tag interference is high when the number of parallel backscatter transmissions is large.

**Frequency & Time Offset.** Normally, the peak will appear in the center of each FFT bin. However, different tags have different ToF to the gateway. This leads to peak drift in the FFT result, i.e., the peak no longer locates in the center of the bin. The peak drift can result in decoding error in practice, e.g., a bit “1” sent by tag  $n$  can be shifted to the FFT bin allocated for tag  $n + 1$ , which actually sends bit “0”.

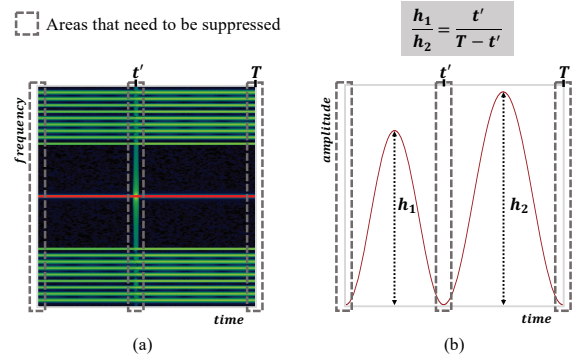


Figure 10: (a) Frequency leakage at the splicing position. (b) Our design of window function to suppress the frequency leakage.

**Near-far Problem.** Each backscatter signal will produce leakage in the frequency domain after FFT, known as sidelobes. A strong backscatter signal, which produces sidelobes with high amplitude, can mask adjacent weaker peaks.

To address time and frequency offset, we add empty FFT bins between two allocated bins. The number of empty bins should be carefully set. On one hand, we should place as many empty FFT bins as possible to tolerate time & frequency offsets and the near-far problem. On the other hand, to achieve minimal spectrum consumption, we must compress the spacing between adjacent allocated FFT bins. In our implementation, we select nine empty FFT bins between two allocated bins. Netscatter [6] adopts one empty FFT bin to enable higher concurrency. It uses more complex tags to detect the signal strength of the excitation signal and dynamically adjust the backscatter power. The received hybrid signal consists of multiple backscatter chirps; after dechirp, the signal transforms to multiple single-tone signals at different frequencies. Figure 10(a) plots the time-frequency representation of the excitation signal and backscatter signals after dechirp.  $t'$  represents the phase jumping time. The red line indicates the excitation signal and the green lines are the backscatter signals spaced with nine bins. We also leave some spacing frequency between the red line and the green lines to reduce the interference of the excitation signal.

To address the inter-tag interference, we need to mitigate the impact of sidelobes on other peaks. For the FFT, the two endpoints of the time waveform are interpreted as though they were connected together [16]. In most cases, the phases at the two endpoints of the signal are different, which introduces sharp discontinuity of phase and frequency leakage at the adjacent frequency band, i.e., higher sidelobes. A classic way to solve the sidelobe problem is using a window function. We should carefully design the window to balance the effectiveness of sidelobe elimination and SNR loss. In our design, we use the Hanning window. A Hanning window smoothly reduces the amplitude of the signal towards zero from the center to two edges. Therefore, it decreases the sharp phase discontinuity. As mentioned above, there is a phase jumping at the splicing point. Thus, solely using the original Hanning window is not adequate. Besides the two end points of the signal, the position of the phase jumping also needs to be suppressed, as shown in Figure 10(a). In

practice, the position  $t'$  of the phase jumping can be inferred from the decoded data of the excitation signal. To suppress the phase discontinuity at  $t'$ , we design a window function consisting of two Hanning windows as shown in Figure 10(b). We also find that if  $t'$  or  $T - t'$  is much less than  $T$ , the amplitude of the signal in the shorter window will change drastically, which causes additional frequency leakage. To avoid the sharp changing of the amplitude, we set different scaling factors to those two Hanning windows. We choose the scaling factor proportional to the window length, *i.e.*,  $\frac{h_1}{h_2} = \frac{t'}{T-t'}$  as shown in Figure 10(b). After applying the specially designed window to the signal, we can effectively mitigate the inter-tag interference. This is also validated in our experiment results in Section 7.4.2.

## 6 IMPLEMENTATION

We prototype P<sup>2</sup>LoRa on a customized printed circuit board (PCB). The wake-up module consists of a three-stage voltage-doubling amplifier HSMS-285C [17] and a low-power voltage comparator LPV7215MG [18]. The controller is a STM32L011D3P6 [19] MCU which controls a low-power DAC MAX5530 [20] and a low-power DCO LTC6990IS6 [21] to output baseband signal. A reflective RF switch ADG902 [22] modulates the baseband signal and transmits the backscatter signal through a 4 dBi gain omnidirectional antenna. The total power consumption of our backscatter tag, including the waking-up unit and backscatter modulation unit, is only 320  $\mu$ W.

The RF source is a COTS LoRa node with a Semtech SX1276 [23] radio chip and a 4 dBi gain omnidirectional antenna. The gateway is a USRP N210 [24] with a UBX daughter board and a 3 dBi gain omnidirectional antenna. Both of them operate at the 433 MHz band. (Previous works use 900 MHz band, which contains strong interference in our experimental area.) Since our decoding algorithm only requires I/Q samples, it can also be implemented on other commercial LoRa chipsets, *e.g.*, SX1257 [25]. We use the UHD+GNU-Radio library for our hybrid signal demodulator and implement P<sup>2</sup>LoRa in MATLAB to process the I/Q samples offline.

## 7 EVALUATION

### 7.1 Comparison with Existing Works

We compare P<sup>2</sup>LoRa with the following two ambient backscatter systems.

- PLoRa [7]: Ambient LoRa backscatter by shifting LoRa signal out of band.
- Aloba [8]: Ambient LoRa backscatter with OOK modulation.

To fully evaluate the performance of canceling interference of excitation signal and concentrating double sideband energy, we implement a version of P<sup>2</sup>LoRa without these two operations, namely P<sup>2</sup>LoRa-.

The default setting of LoRa used in our experiment: SF = 12, BW = 500 kHz, coding rate =  $\frac{4}{5}$ , and transmission power = 20 dBm. P<sup>2</sup>LoRa applies 2-FSK modulation at 254 kHz and 256 kHz, respectively. The switching rate of Aloba is set to 10 kHz, which achieves the longest communication distance in their system. The SF of backscatter signals is the same as that of the excitation signals in our experiments. We measure the BER (bit error rate) and throughput with different source-to-tag ( $d_{ST}$ ), tag-to-receiver ( $d_{TR}$ ), source-to-receiver ( $d_{SR}$ )

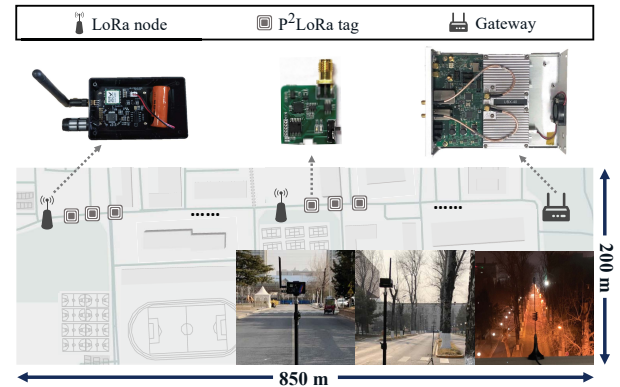


Figure 11: Outdoor experiment map.

distances in both indoor and outdoor environments. The LoRa node sends 800 packets for each distance, and the backscatter tag piggybacks 32 bits payload into each LoRa packet. For demonstration, if all data bits are successfully received, we mark BER as  $10^{-4}$  in the figures.

**7.1.1 Outdoor scenario.** As shown in Figure 11, we place the receiver at a fixed position of an open road then move the LoRa node (source) and the backscatter tag from 50 m to 850 m. Figure 12 shows that the BER of P<sup>2</sup>LoRa is lower than that of the other two systems for all settings. When  $d_{ST} = 1$  m, P<sup>2</sup>LoRa enhances the communication range by 67% compared with PLoRa and 10 $\times$  compared with Aloba. Aloba uses OOK modulation and checks the amplitude and phase characteristics of the signal in the time domain, the accumulated signal energy is very limited, which results in short communication distance. When  $d_{ST} = 5$  m and  $d_{TR} = 100$  m, the BER of Aloba quickly climbs up to 10%. As the communication distance further increases, Aloba soon stops working and cannot transmit any data packets.

As shown in Figure 12(a) and Figure 12(b), when  $d_{ST} = 1$  m and 5 m, P<sup>2</sup>LoRa supports 500 m and 400 m backscatter range with a low BER, while PLoRa has the BER of around 10% at similar settings. The performance enhancement of P<sup>2</sup>LoRa comes from the following aspects: First, the concentration of the upper and lower sidebands provides a gain of 1-2 dB. Second, P<sup>2</sup>LoRa compensates for the phase jumping in the received signal for FFT, while the phase in PLoRa jumps twice and is not compensated. Therefore, PLoRa experiences more SNR loss. In addition, P<sup>2</sup>LoRa performs the splicing operation on the gateway in the digital domain, while PLoRa does it on tags in the analog domain. Consequently, the splicing operation of PLoRa is more susceptible to frequency mismatch under the presence of temperature differences. The environment where we calibrate the crystal oscillator of the backscatter tag has a large temperature difference with the outdoor environment (around 20  $^{\circ}$ C). This will hamper the concentration of the whole symbol energy, which further incurs SNR loss for PLoRa. Third, PLoRa uses two antennas to shift the excitation signal simultaneously. The distance between the antennas is close (*e.g.*, 5 cm), and the coupling effect [26] between the antennas leads to SNR loss.

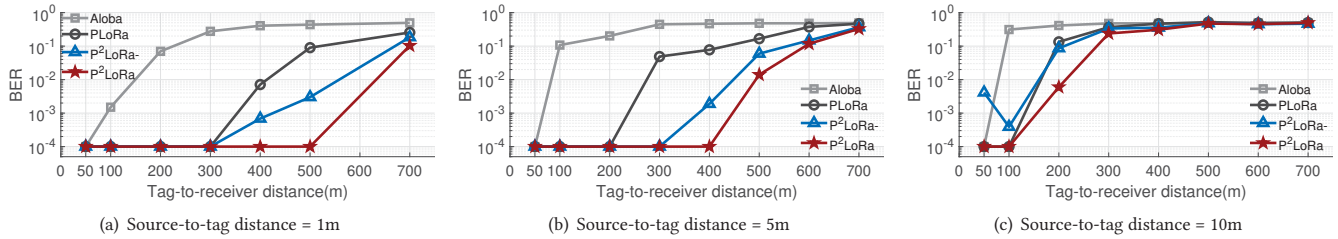


Figure 12: BER comparison of P<sup>2</sup>LoRa, PLoRa and Aloba in different source-to-tag distance with SF12 in outdoor scenario.

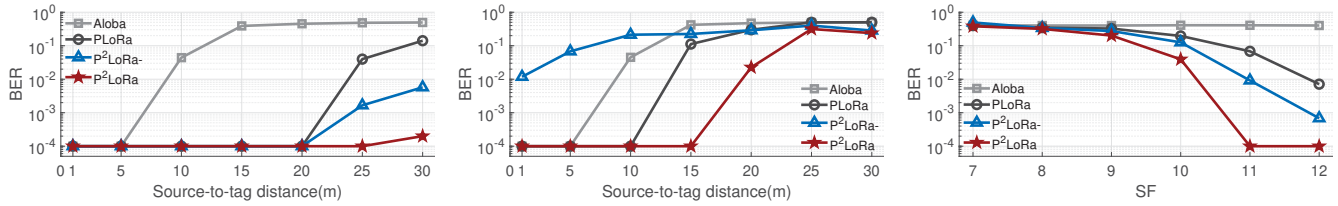


Figure 13: BER comparison with SF12 (indoor).

Figure 14: BER comparison with SF8 (indoor).

Figure 15: BER comparison with different SF (outdoor).

We also examine that our interference-canceling operation can provide significant improvements in decoding. For different distance, the BER of P<sup>2</sup>LoRa is always lower than that of PLoRa-. As P<sup>2</sup>LoRa- also benefits from our splicing methods, it achieves a lower BER than PLoRa and Aloba, except for the scenario when  $d_{ST} = 10\text{ m}$  and  $d_{TR} \leq 100\text{ m}$ , as shown in Figure 12(c). In this scenario, the source is relatively close to the receiver and is distant to the tag. Thus, the interference from the excitation signal is relatively strong to the backscatter signal. Comparing the performance of P<sup>2</sup>LoRa- with  $d_{TR} = 50\text{ m}$  and  $d_{TR} = 100\text{ m}$  in Figure 12(c), we can find an interesting phenomenon that the BER of P<sup>2</sup>LoRa- under  $d_{TR} = 50\text{ m}$  is even higher than the BER under  $d_{TR} = 100\text{ m}$ . We can see that as  $d_{TR}$  increases, the interference from the excitation signal gradually becomes weaker. When  $d_{TR}$  reaches 100 m, the power of interference attenuates and the BER of P<sup>2</sup>LoRa- quickly drops. Comparing the BER result of P<sup>2</sup>LoRa with PLoRa-, we can see that the interference canceling operation ensures the stable BER performance of P<sup>2</sup>LoRa.

**7.1.2 Indoor scenario.** We then compare the BER of the above three backscatter systems in an office building. As shown in Figure 16, we place the gateway in the corner of the room and place the LoRa node outside the room. The gateway receives the signal from the tag and the LoRa node. We fix the position of the tag and move the LoRa node along the corridor. Then, we set  $d_{TR}$  to 12 m and change  $d_{ST}$  from 1 m to 30 m. Both the original LoRa signal and the backscatter signal would propagate through a wall to the gateway in the experiment setting.

As shown in Figure 13, when  $d_{TR} = 30\text{ m}$ , the BER of P<sup>2</sup>LoRa remains less than  $10^{-3}$  while the BER of PLoRa increases to 4%. Aloba shows a more vulnerable link quality. When  $d_{ST} = 10\text{ m}$ , the BER of Aloba reaches 4.4%, and Aloba stops working when the distance reaches 15 m. This reveals that compared with PLoRa and

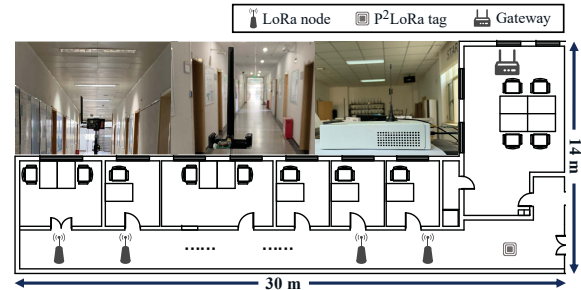


Figure 16: Indoor experiment map.

Aloba, P<sup>2</sup>LoRa is more robust and can achieve better performance to support indoor sensing and communication.

**7.1.3 Impact of SF.** In order to verify the BER performance under excitation signals with different parameters, we test the performance for SF from 7 to 12. The result of SF8 in indoor environments is shown in Figure 14. A smaller SF corresponds to lower sensitivity in LoRa modulation. Thus P<sup>2</sup>LoRa only reaches  $d_{ST} = 15\text{ m}$  with SF8. In this experiment, we have another interesting observation: P<sup>2</sup>LoRa- has a lower performance than PLoRa and Aloba. Comparing Figure 13 and Figure 14, P<sup>2</sup>LoRa- shows stable performance under SF12. We investigate the data and find that the phenomenon comes from the in-band frequency leakage caused by the excitation signal. When a LoRa chirp experiences the frequency discontinuity (e.g., from the upper bandwidth limit to the lower), the leakage will span the whole frequency band and interfere the backscatter signal. The smaller the SF, the higher the proportion of the discontinuous area in the entire signal, which means stronger interference. Nevertheless, after the interference canceling operation, P<sup>2</sup>LoRa significantly suppresses the frequency leakage and reduces the BER

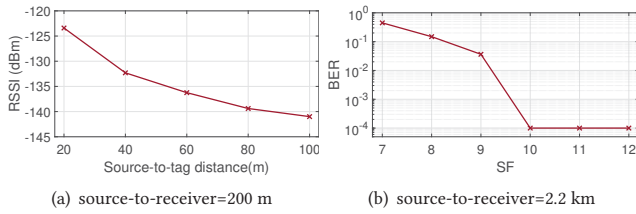


Figure 17: RSSI of backscatter signals under different  $d_{ST}$ .

by 75%. We set  $d_{ST} = 1$  m and receive the signal at 400 m. Then, we measure the BER under different SFs. As shown in Figure 15, P<sup>2</sup>LoRa and PLoRa achieve a lower BER with a larger SF. Without the interference cancellation, the BER of P<sup>2</sup>LoRa- is similar to (even worse than) Aloha and PLoRa for SF7 and SF8. These results show that P<sup>2</sup>LoRa is compatible with various SF settings and can achieve a robust performance.

## 7.2 In-band Interference Suppression

The backscatter signals in our system share the spectrum with the excitation signal, which brings severe in-band interference. We measure the signal strength of the excitation signal and its impact on the backscatter signal with various  $d_{SR}$  in both indoor and outdoor scenarios. P<sup>2</sup>LoRa suppresses the interference of excitation signal by the following aspects: First, the backscatter signal is shifted by at least  $\frac{BW}{2}$ . The sidelobes of the excitation signal are gradually decreased as the shifting frequency increases. Second, our cancellation technique constructs the excitation signal in the digital domain and then cancels it from the hybrid signal. For different  $d_{SR}$  in the outdoor environment, the total suppressed SNR is around 72 dB. Even in the indoor environment with complex multipath interference, the suppression performance is close to that in the outdoor environment. Therefore, the suppressed sidelobes of the excitation signal will not cause notable interference to the backscatter signal demodulation.

## 7.3 Long Range Experiments

**7.3.1 Long source-to-tag distance.** In this experiment, we use the excitation signal with SF = 12 and BW = 31.25 kHz. The transmission power of the excitation signal is set to 30 dBm. We fix  $d_{SR} = 200$  m and move the tag between the LoRa node and the gateway. We measure the signal strength of the backscatter signal at different  $d_{ST}$ . As shown in Figure 17(a), the signal strength of the backscatter signal decreases with increasing of  $d_{ST}$ . In the backscatter link, the SNR reaches its lowest at the midpoint of the transmitter and receiver (i.e.,  $d_{ST} = d_{TR}$ ) [5] [27]. We can see that even when  $d_{ST} = 100$  m, the backscatter data packet can still be received. When  $d_{ST}$  further increases, our wake-up circuit cannot reliably wake up the backscatter tag. Currently, the performance bottleneck of P<sup>2</sup>LoRa is the wake-up sensitivity, and we plan to improve this in our next version. Nevertheless, our design can support moving the tag to any position between the source and receiver with  $d_{SR} = 200$  m, which meets the requirements of many applications.

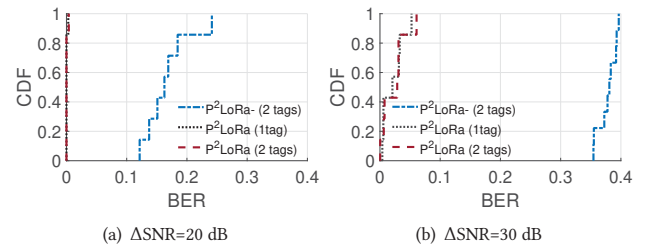


Figure 18: BER with different  $\Delta$ SNR.

**7.3.2 Long tag-to-receiver distance.** In this experiment, we test the performance for long tag-to-receiver distance. We set BW = 500 kHz and the transmission power of the excitation signal to 30 dBm. Typically, using a smaller bandwidth can increase the distance as this concentrates the energy to a smaller spectrum. As the largest diameter of our experimental field is only 2.2 km, we do not require the bandwidth to be as narrow as that in Section 7.3.1. We put the backscatter tag close to the LoRa node and the receiver 2.2 km to the LoRa node. Then we measure the BER of the backscatter signal under different SFs. As shown in Figure 17(b), when the SF is larger than 9, P<sup>2</sup>LoRa successfully transmits all data bits. Thus, P<sup>2</sup>LoRa can achieve a reliable transmission range of 2.2 km. The received BER also suggests if a smaller bandwidth is used, the coverage of the network can be further extended.

## 7.4 Parallel Decoding

In this section, we examine the parallel transmission performance of P<sup>2</sup>LoRa. We first examine different impacting factors to parallel decoding and then show the overall parallel decoding performance.

**7.4.1 Near-far problem.** We measure the maximum allowable power difference between tags, which also shows the robustness to the near-far problem. We assign two adjacent shifting frequencies to tag #1 and tag #2, and then place them with the same distance to the RF source. Then, we connect tag #2 to a step attenuator, continuously reduce its transmitting signal power and record the BER for the cases when tag #1 transmits and does not transmit. In order to show the reduction of inter-tag interference, we also measure the BER in two different scenarios for comparison: (1) our specially designed window function is not used which is marked as P<sup>2</sup>LoRa- (2 tags), and (2) the tag with stronger signal strength is removed, which is marked as P<sup>2</sup>LoRa (1 tag) in Figure 18.

We define the difference between the SNR before and after connecting to the attenuator as  $\Delta$ SNR. As shown in Figure 18, when  $\Delta$ SNR= 20 dB, regardless of whether there exists interference from the stronger tag, the overall BER of P<sup>2</sup>LoRa is very low (close to 0). However, the overall BER of P<sup>2</sup>LoRa- is between 10% and 25%. This is because under the strong interference, a portion of bits “0” are distorted into bits “1”, and a portion of bits “1” are masked by the sidelobes of the stronger signal. When the  $\Delta$ SNR is increased to 30 dB, the overall BER of P<sup>2</sup>LoRa- further increases to between 35% and 40%. In those settings, P<sup>2</sup>LoRa still retains a similar BER performance to P<sup>2</sup>LoRa (1 tag). The above experiments show that

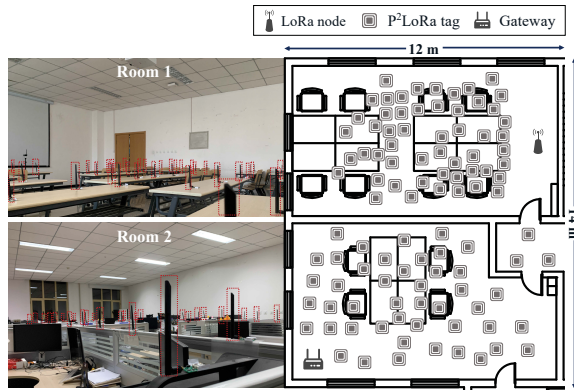


Figure 19: Experiment with 101 backscatter tags.

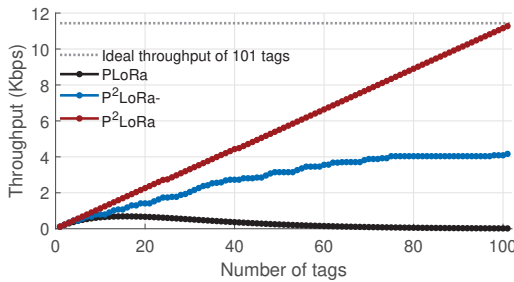


Figure 20: Overall network throughput.

our system provides a dynamic range of at least 30 dB. According to the Friis transmission formula [28], the dynamic range can translate to about  $32\times$  propagation distance difference, which facilitates the deployment of our system on a large scale.

**7.4.2 Deployment in the Field.** Finally, we deploy 101 tags in the office environment as shown in Figure 19. The LoRa node is located in room 1, and the gateway is located in room 2. All tags perform OOK modulation on the allocated frequency. The shifting frequency is pre-allocated to each tag. We use  $BW=500$  kHz and  $SF=12$  for the LoRa transmission. The maximum shifting frequency is around  $\frac{3}{4}BW$ . All tags are randomly placed in those two rooms. Therefore, tags with adjacent FFT bins are likely to be in positions with different RF environments.

**Overall Network Throughput.** In this experiment, we start with only one tag and gradually increase the number of tags to 101. Every time a tag is added to the network, we measure the overall throughput. Here, we also test the performance of P²LoRa for comparison.

As shown in Figure 20, the overall throughput of P²LoRa increases approximately linearly with the increase of the number of tags. The throughput reaches 11.27 kbit/s for 101 tags, which is close to the ideal maximum throughput rate of 11.44 kbit/s. In contrast, the throughput of PLoRa- only reaches 4.49 kbit/s for 101 tags. It shows poor scalability as the number of tags increases. When the number of tags increases to 75, further increase of the

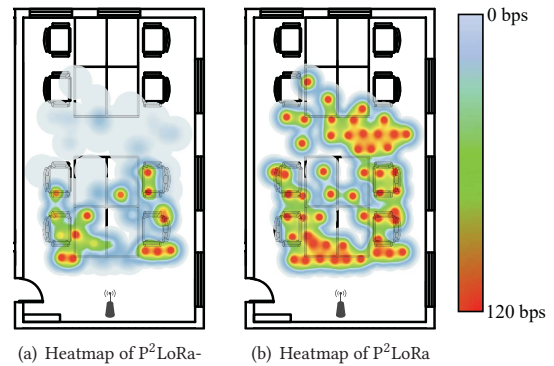


Figure 21: Throughput heatmap before and after interference cancellation.

tags brings no throughput enhancement to P²LoRa- due to inter-tag interference. PLoRa mentions that it can run the frequency domain ALOHA protocol to mitigate collisions among tags. Thus, we allocate 16 channels for PLoRa (Note that in our experiment, the extra spectrum occupied by P²LoRa is even less than two channels). When the number of tags is 16, PLoRa reaches the maximum throughput of 0.69 kbit/s. Once the number of tags exceeds the number of available channels, collisions among tags inevitably increase and the throughput accordingly decreases. PLoRa can only achieve a throughput of 0.019 kbit/s for 101 tags due to inter-tag interference.

**Throughput of individual tags.** In real system deployments, we also observe obvious inter-tag interference. As shown in Figure 21, we measure the throughput of each tag in room 2 with/without inter-tag interference cancellation. Without inter-tag interference cancellation, tags of high throughput are usually located in the area close to the RF source. Tags far away from the RF source only achieve a low throughput. There are also many blind spots in P²LoRa- where the throughput of tags in those areas is significantly reduced. With inter-tag interference cancellation, all tags in room 2 demonstrate a high throughput, as shown in Figure 21(b). The window function suppresses the strong interference from other tags in the room and clears the previous blind spots.

### 7.5 Impact to Normal LoRa Transmissions

We keep  $d_{SR} = 500$  m and  $d_{SR} = 700$  m, and then add different numbers of P²LoRa tags in the network to explore the impact of backscatter signals to the packet reception rate (PRR) of normal LoRa packets. The receiver in this experiment is a commercial LoRa gateway with SX1276. P²LoRa tags are placed near the LoRa node or the LoRa gateway (less than 1m) to maximize the interference of the backscatter signal.

P²LoRa uses frequency shifting-based modulation, and it does not corrupt the peak characteristics of LoRa in the frequency domain. Meanwhile, the backscatter signal is typically orders of magnitude weaker than the original LoRa signal. As shown in Figure 22, when  $d_{SR} = 500$  m, regardless of the number of backscatter tags, the PRR of normal LoRa transmission is close to 100%. As  $d_{SR}$  increases

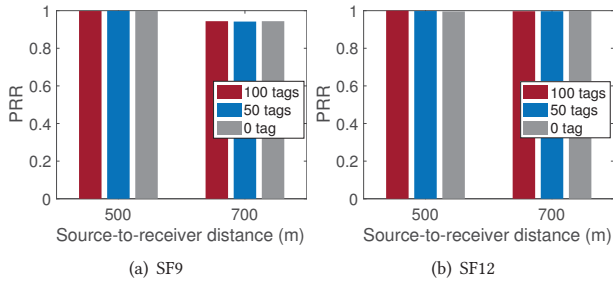


**Figure 22: Impact of backscatter signal to normal LoRa transmission.**

to 700 m, the PRR of normal LoRa for SF9 with no backscatter interference is around 94.4%. After turning on 50 or 100 backscatter tags, it can still achieve a similar PRR. This result demonstrates that the impact of P<sup>2</sup>LoRa to normal LoRa transmission is negligible.

## 8 RELATED WORKS

**Wi-Fi, TV, and FM backscatter.** Ambient backscatter [29] uses ambient TV or cellular signals as the excitation signal for communication. FM backscatter [30] reflects the ambient FM signal and embeds data over it. Wi-Fi backscatter [31] reuses the existing Wi-Fi infrastructure to convey data bits by varying the RSSI of Wi-Fi packets. BackFi [32] changes the phase of the incoming Wi-Fi signal to convey data bits. WiTag [27] selectively corrupts some of the subframes in a Wi-Fi packet and checks the ACK of each subframe to decode the backscatter signal. However, the communication range of the above technologies is limited to several meters. Hitchhike [14] piggybacks data on a Wi-Fi packet by translating the original 802.11b codeword to another valid codeword. Interscatter [33] uses a single-tone signal sent by a BLE device as the excitation signal and generates a legitimate Wi-Fi signal. In order to scale the passive network, OFDMA backscatter [34] and Digiscatter [35] enable OFDMA in Wi-Fi backscatter. LoRea [36] achieves a communication distance of thousands of meters, but it requires a dedicated RF source providing a single-tone signal.

**LoRa backscatter.** To improve the communication range, LP-WAN technology such as LoRa [9], is exploited in backscatter communication. PLoRa [7] uses ambient LoRa transmission as the excitation signal and uses two baseband signals to modulate chirps with different shifting frequencies. They cannot effectively support parallel backscattering. PolarScatter [37] exploits channel polarization to achieve a high communication distance and throughput. It requires a dedicated encoder which costs extra power budget. LoRa backscatter [5] and Netscatter [6] use a single-tone excitation signal, and the backscatter tag modulates the excitation signal to the chirp signal. They require complex signal operations at backscatter tags, and therefore increase the deployment and maintenance overhead. Aloha [8] improves the throughput of PLoRa by proposing a OOK-like backscatter modulation method. However, it can only support a very limited number of concurrent backscatter tags and can only reach a communication distance of 250 m.

**Parallel backscatter/LoRa decoding.** Parallel decoding addresses the collisions among data packets and is widely used in

active and passive networks. FlipTracer [38] adopts a transition probabilities model to separate collided backscatter packets. As the number of tags increases, the decoding difficulty of FlipTracer increases exponentially; therefore, it only supports five parallel tags according to their experiments. Aloha [8] follows a similar decoding algorithm of FlipTracer and thus has a similar shortage. Netscatter [6] assigns an FFT bin to each tag for OOK modulation. However, it uses a dedicated RF source generating excitation signals rather than ambient LoRa transmission. Choir [39] exploits the inherent frequency imperfection feature of LoRa nodes to separate concurrent LoRa transmissions. However, the resolution of Choir in frequency is not enough to achieve parallel decoding when the number of tags increases. mLoRa [40] and FTrack [41] use the misaligned edges of LoRa chirps to separate multiple active LoRa packets. CoLoRa [15], Nscale [12], and Pyramid [42] track the peak feature in the frequency domain to distinguish and separate collisions in the active LoRa network. Essentially, the above systems use the time difference among different data packets. Those systems are unsuitable for our design, as the backscatter tags are usually synchronized with very small time misalignment.

## 9 CONCLUSION

We present P<sup>2</sup>LoRa, the first ambient LoRa backscatter system with parallel decoding and long-range communication. The basic idea of P<sup>2</sup>LoRa is to shift the ambient LoRa packet with a small frequency. We address several key challenges to achieve a long-range communication with parallel decoding. We reveal the leaked energy in traditional backscatter systems and enhance the SNR of the backscatter signal by concentrating leaked energy in the sidebands. We propose a method to accurately reconstruct and cancel the in-band excitation signal which is orders of magnitude higher than the backscatter signal. For parallel decoding, we leverage the combined Hanning window to cancel the inter-tag interference with very low overhead. We prototype P<sup>2</sup>LoRa tag with customized hardware components and implement the gateway on the SDR platform. We extensively evaluate the performance of P<sup>2</sup>LoRa under different environments. The results show that P<sup>2</sup>LoRa can achieve a long communication range of 2.2 km with ambient LoRa as the excitation signal and supports 101 parallel tag transmissions.

## 10 ACKNOWLEDGMENTS

We thank the anonymous shepherd and reviewers for their insightful comments to improve the quality of our work. This work is in part supported by NSFC No. 61932013 and Tsinghua-Foshan Innovation Special Fund (TFISF). Jiliang Wang is the corresponding author.

## REFERENCES

- [1] SEMTECH. LoRa applications. <https://www.semtech.com/lora/lora-applications>.
- [2] Rajalakshmi Nandakumar, Vikram Iyer, and Shyamnath Gollakota. 3d localization for sub-centimeter sized devices. In *Proceedings of ACM Sensys*, 2018.
- [3] Atul Bansal, Akshay Gadre, Vaibhav Singh, Anthony Rowe, Bob Iannucci, and Swarn Kumar. OwLL: Accurate LoRa Localization using the TV Whitespaces. In *Proceedings of ACM/IEEE IPSN*, 2021.
- [4] Yuxiang Lin, Wei Dong, Yi Gao, and Tao Gu. SateLoc: A virtual fingerprinting approach to outdoor LoRa localization using satellite images. *ACM Transactions on Sensor Networks (TOSN)*, 17(4):1–28, July 2021.
- [5] Vamsi Talla, Mehrdad Hesar, Bryce Kellogg, Ali Najafi, Joshua R Smith, and Shyamnath Gollakota. LoRa backscatter: Enabling the vision of ubiquitous

- connectivity. In *Proceedings of ACM UbiComp*, 2017.
- [6] Mehrdad Hesar, Ali Najafi, and Shyamnath Gollakota. Netscatter: Enabling large-scale backscatter networks. In *Proceedings of USENIX NSDI*, 2019.
- [7] Yao Peng, Longfei Shangguan, Yue Hu, Yujie Qian, Xianshang Lin, Xiaojiang Chen, Dingyi Fang, and Kyle Jamieson. PLoRa: A passive long-range data network from ambient LoRa transmissions. In *Proceedings of ACM SIGCOMM*, 2018.
- [8] Xiuzhen Guo, Longfei Shangguan, Yuan He, Jia Zhang, Haotian Jiang, Awais Ahmad Siddiqi, and Yunhao Liu. Aloba: rethinking ON-OFF keying modulation for ambient LoRa backscatter. In *Proceedings of ACM Sensys*, 2020.
- [9] LoRa Alliance. LoRa. <https://loro-alliance.org/>.
- [10] WISP. <https://sites.google.com/uw.edu/wisp-wiki/home>.
- [11] Bryce Kellogg, Vamsi Talla, Shyamnath Gollakota, and Joshua R Smith. Passive wi-fi: Bringing low power to wi-fi transmissions. In *Proceedings of USENIX NSDI*, 2016.
- [12] Shuai Tong, Jiliang Wang, and Yunhao Liu. Combating packet collisions using non-stationary signal scaling in LPWANS. In *Proceedings of ACM MobiSys*, 2020.
- [13] Olivier Bernard André Seller, Nicolas Sornin. Low complexity, low power and long range radio receiver, US Patent 10,305,535, 2019.
- [14] Pengyu Zhang, Dinesh Bharadia, Kiran Joshi, and Sachin Katti. Hitchhike: Practical backscatter using commodity WiFi. In *Proceedings of ACM Sensys*, 2016.
- [15] Shuai Tong, Zhenqiang Xu, and Jiliang Wang. CoLoRa: Enabling Multi-Packet Reception in LoRa. In *Proceedings of IEEE INFOCOM*, 2020.
- [16] National Instruments. Understanding FFTs and Windowing. <https://download.ni.com/evaluation/pxi/Understanding%20FFTs%20and%20Windowing.pdf>.
- [17] Avago. HSMS-285C. <https://docs.broadcom.com/doc/AV02-1377EN>.
- [18] Texas Instruments. LPV7215MG. <https://www.ti.com/store/ti/en/p/product/?p=LPV7215MG/NOPB>.
- [19] STMicroelectronics. STM32L011D3P6. <https://www.st.com/resource/en/datasheet/stm32l011d4.pdf>.
- [20] Maxim. MAX5530. <https://datasheets.maximintegrated.com/en/ds/MAX5530-MAX5531.pdf>.
- [21] Analog Devices. LTC6990IS6. <https://www.analog.com/media/en/technical-documentation/data-sheets/LTC6990.pdf>.
- [22] Analog Devices. ADG902. [https://www.analog.com/media/en/technical-documentation/data-sheets/ADG901\\_902.pdf](https://www.analog.com/media/en/technical-documentation/data-sheets/ADG901_902.pdf).
- [23] Semtech. SX1276. <https://www.semtech.com/products/wireless-rf/loro-transceivers/sx1276>.
- [24] Ettus Research. USRP N210. <https://www.ettus.com/all-products/un210-kit/>.
- [25] Semtech. Data Sheet SX1257, Rev. 1.2, 2018.
- [26] Zhongqin Wang, Min Xu, Ning Ye, Haiping Huang, Ruchuan Wang, and Fu Xiao. RF-Mirror: Mitigating Mutual Coupling Interference in Two-Tag Array Labeled RFID Systems. In *Proceedings of IEEE SECON*, 2020.
- [27] Ali Abedi, Farzan Dehbashi, Mohammad Hossein Mazaheri, Omid Abari, and Tim Brecht. Witag: Seamless wifi backscatter communication. In *Proceedings of ACM SIGCOMM*, 2020.
- [28] Harald T Friis. A note on a simple transmission formula. *Proceedings of the IRE*, 34(5):254–256, 1946.
- [29] Vincent Liu, Aaron Parks, Vamsi Talla, Shyamnath Gollakota, David Wetherall, and Joshua R Smith. Ambient backscatter: Wireless communication out of thin air. In *SIGCOMM*. ACM, 2013.
- [30] Anran Wang, Vikram Iyer, Vamsi Talla, Joshua R Smith, and Shyamnath Gollakota. {FM} backscatter: Enabling connected cities and smart fabrics. In *Proceedings of USENIX NSDI*, 2017.
- [31] Bryce Kellogg, Aaron Parks, Shyamnath Gollakota, Joshua R Smith, and David Wetherall. Wi-Fi backscatter: Internet connectivity for RF-powered devices. In *Proceedings of ACM SIGCOMM*, 2014.
- [32] Dinesh Bharadia, Kiran Raj Joshi, Manikanta Kotaru, and Sachin Katti. Backfi: High throughput wifi backscatter. In *Proceedings of ACM SIGCOMM*, 2015.
- [33] Vikram Iyer, Vamsi Talla, Bryce Kellogg, Shyamnath Gollakota, and Joshua Smith. Inter-technology backscatter: Towards internet connectivity for implanted devices. In *Proceedings of ACM SIGCOMM*, 2016.
- [34] Renjie Zhao, Fengyuan Zhu, Yuda Feng, Siyuan Peng, Xiaohua Tian, Hui Yu, and Xinbing Wang. OFDMA-enabled Wi-Fi backscatter. In *Proceedings of ACM MobiCom*, 2019.
- [35] Fengyuan Zhu, Yuda Feng, Qianru Li, Xiaohua Tian, and Xinbing Wang. DigiS-catter: efficiently prototyping large-scale OFDMA backscatter networks. In *Proceedings of ACM MobiSys*, 2020.
- [36] Ambuj Varshney, Oliver Harms, Carlos Pérez-Penichet, Christian Rohner, Fredrik Hermans, and Thiemo Voigt. LoRea: A backscatter architecture that achieves a long communication range. In *Proceedings of ACM Sensys*, 2017.
- [37] Guochao Song, Hang Yang, Wei Wang, and Tao Jiang. Reliable wide-area backscatter via channel polarization. In *Proceedings of IEEE INFOCOM*, 2020.
- [38] Meng Jin, Yuan He, Xin Meng, Yilun Zheng, Dingyi Fang, and Xiaojiang Chen. Fliptracer: Practical parallel decoding for backscatter communication. In *Proceedings of ACM MobiCom*, 2017.
- [39] Rashad Eletreby, Diana Zhang, Swarn Kumar, and Osman Yağan. Empowering low-power wide area networks in urban settings. In *Proceedings of ACM SIGCOMM*, 2017.
- [40] Xiong Wang, Linghe Kong, Liang He, and Guihai Chen. mLoRa: A multi-packet reception protocol in LoRa networks. In *Proceedings of IEEE ICNP*, 2019.
- [41] Xianjin Xia, Yuanqing Zheng, and Tao Gu. Ftrack: Parallel decoding for lora transmissions. In *Proceedings of ACM Sensys*, 2019.
- [42] Zhenqiang Xu, Pengjin Xie, and Jiliang Wang. Pyramid: Real-Time LoRa Collision Decoding with Peak Tracking. In *Proceedings of IEEE INFOCOM*, 2021.